J. Fluid Mech. (2007), *vol.* 587, *pp.* 23–44. © 2007 Cambridge University Press
doi:10.1017/S0022112007007264 Printed in the United Kingdom

Quasi-static rheology of foams. Part 1. Oscillating strain

ALEXANDRE KABLA[1] AND GEORGES DEBREGEAS[2]

[1]Department of Engineering, University of Cambridge, Trumpington Street, Cambridge, CB2 1PZ, UK

[2]Laboratoire de Physique Statistique, Ecole Normale Supérieure, CNRS – UMR 8550, 24 Rue Lhomond, 75231 Paris Cedex 05, France

(Received 23 May 2006 and in revised form 29 April 2007)

A quasi-static simulation is used to study the mechanical response of a disordered bidimensional aqueous foam submitted to an oscillating shear strain. The application of shear progressively extends the elastic domain, i.e. the strain range within which no plastic process occurs. It is associated with the development of an irreversible normal stress difference, and a decrease in the shear modulus, which are both signatures of the appearance of anisotropy in the film network. Beyond this mechanical measurement, the evolution of the structural properties of the foam is investigated. We focus in particular on the energy E_0 defined as the minimum line-length energy under zero shear stress. For strain amplitude less than $\sim$0.5, this quantity is found to decay with the number of applied cycles as a result of the curing of topological defects. However, for higher strain amplitude, plastic events appear to increase the structural disorder and tend to gather near the shearing walls. This process is a precursor of the shear-banding transition observed in fully developed flows, which will be studied in the companion paper. Movies are available with the online version of the paper.

1. Introduction

The rheology of soft glasses has been the subject of an increasing number of studies in the last two decades. This class of systems includes macroscopically divided materials such as foams, concentrated emulsions, colloidal suspensions or dense granular packings, but also multicontact frictional joints (Baumberger & Caroli 2006) or dense assemblies of vertices in class II superconductors (Fisher, Fisher & Huse 1991). As in a molecular glass below T_g, the thermal energy in these systems is low compared to the energy barriers for structural relaxation. In the case of macroscopically divided systems such as foams, the thermal energy is effectively zero: in the absence of external stress, the system is trapped in a metastable configuration. (by contrast with glassy systems, where ageing refers to thermally induced dynamics, the same term is used for foams to describe non-thermal effects, such as coarsening, coalescence or drainage). This results in the existence of a finite yield stress below which the material responds elastically. When a larger stress is imposed, it triggers a series of plastic events which release the applied stress, yielding a macroscopic flow.

This particular mode of stress relaxation has a number of rheological consequences. First, it allows for the existence of a quasi-static regime of flow when the inverse of the strain rate is much larger than the relaxation time associated with the plastic event (Khan, Schnepper & Armstrong 1988; Rouyer, Cohen-Addad & Holler 2005). In this

regime, the stress/strain curve shows an initial quasi-linear regime. Beyond this initial charge, the stress signal, measured on small systems, is intermittent: it exhibits a series of linear increases interrupted by rapid drops associated with the successive plastic events. Another characteristic feature of these systems is the so-called strain-induced ageing process: the dynamical properties continuously vary with the application of a moderate shear (Viasnoff & Lequeux 2002). This indicates that even a low strain can trigger a few plastic events which modify the microscopic structure, that controls, in turn, the macroscopic mechanical response (Bureau, Baumberger & Caroli 2002).

Numerous models have been proposed to interpret this set of observations. Some of them, inspired or derived from glass theory, introduce a parameter which plays the role of a temperature in order to recover a thermodynamical description (Sollich *et al.* 1997; Liu & Nagel 1998). This so-called 'effective temperature' is generally described as a function of the flow field itself. It results in a shear dependent fluidity which has been directly postulated in Derec, Ajdari & Lequeux (2001). Although such models may reproduce the phenomenology of the rheology, they lack a convincing description of the local mechanisms which would justify the proposed form for the effective temperature and its coupling with the flow. An alternative approach, inspired by the pioneering work of Bulatov & Argon (1994*a–c*), has been proposed by Falk & Langer (1998). They observe in a numerical simulation of amorphous and athermal systems of interacting spheres, that plasticity is associated with discrete and local rearrangements involving a few particles. This observation is at the base of the STZ (shear transformation zone) model, which links a microscopic description of the plastic event to the macroscopic rheology. All these models aim to relate the micro-structural state and its evolution with the applied strain and strain rate. A system where one can follow both the micro-structure and the rheology is required in order to further test and refine these different approaches.

Liquid foams constitute a convenient model system to study plasticity in solid materials. It allows us to monitor directly the deformation of a crystalline or disordered structure at the level of its individual components, as was first recognized by Bragg & Nye (1947) who used crystalline bubble rafts as a tool for understanding the dynamics of dislocations in metals. Foam coarsening – the bubble disproportionation induced by gas diffusion between neighbouring bubbles – can be viewed as a process analogous to grain growths in metals (Weaire & Kermode 1984). Disordered foams have proved to be a rich heuristic system for the study of glassy rheology (Sollich *et al.* 1997; Liu & Nagel 1998).

Two-dimensional foams have been particularly investigated both experimentally (Dennin & Knobler 1997; Abd el Kader & Earnshaw 1999; Debrégeas, Tabuteau & di Meglio 2001; Lauridsen, Twardos & Dennin 2002; Cantat & Delannay 2005; Dollet *et al.* 2005) and numerically (Weaire & Kermode 1983; Herdtle & Aref 1992; Okuzono, Kawasaki & Nagai 1993; Reinelt & Kraynik 1996; Kabla & Debrégeas 2003; Vincent-Bonnieu, Hohler & Cohen-Addad 2006) as they allow for simple handling, observation and modelling. Along this line, we have developed a quasi-two-dimensional foam system which consists of a monolayer of bubbles confined between two horizontal plates (Debrégeas *et al.* 2001). Using a numerical foam simulation, a similar flow behaviour was evidenced in plane parallel shear (Kabla & Debrégeas 2003). In spite of the apparent simplicity of these two-dimensional systems, several aspects of their rheological behaviour are still highly debated (Wang, Krishan & Dennin 2006; Janiaud, Weaire & Hutzler 2006).

In this paper and in Part 2 (Kabla, Schéibert & Debrégeas 2007), we attempt to understand the connection between the mechanical properties and the structural state

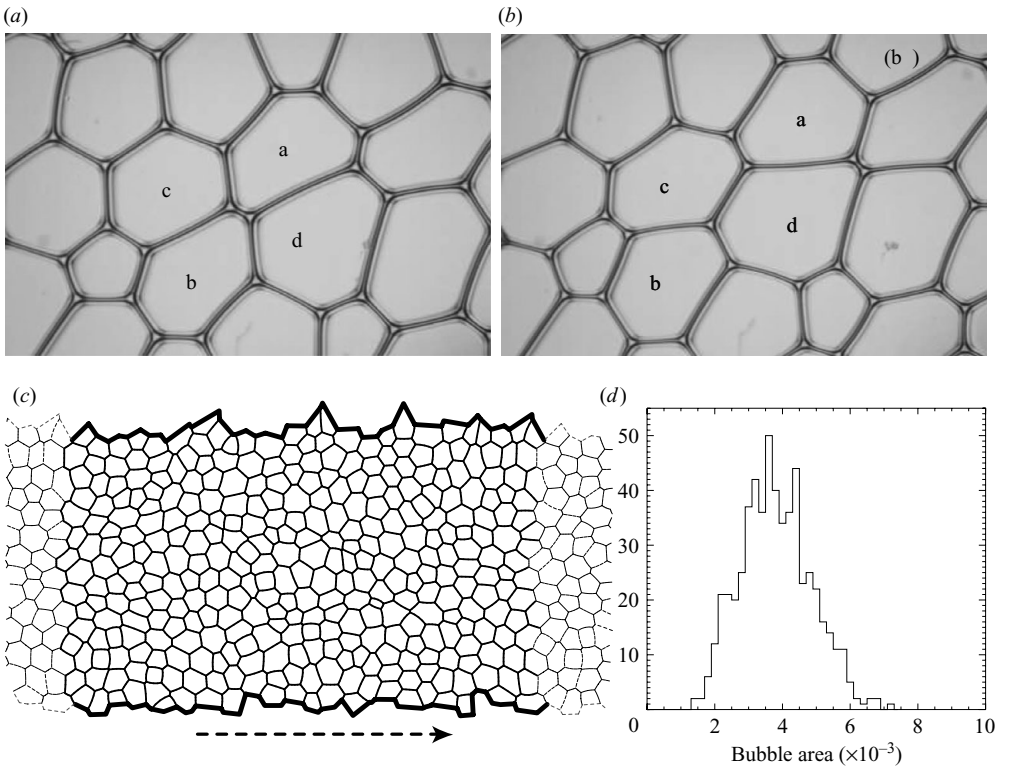

FIGURE 1. (*a*, *b*) A T1 event observed in a confined two-dimensional foam (Debrégeas *et al.* 2001). This elementary plastic process involves a neighbour exchange between 4 bubbles indicated by the letters in the two pictures. (*c*) The numerical two-dimensional foam used in the present study. Shearing is obtained by incrementally moving the lower (rigid) boundary as indicated by the arrow. The foam is periodic along the shear direction. (*d*) Area distribution of the bubbles.

of a foam under two types of solicitation. Following the work of Weaire & Kermode (1984), we study in this paper the response of a foam to an oscillating strain, using the code developed in Kabla & Debrégeas (2003). In Part 2, we investigate fully developed shear flow, experimentally and numerically.

2. Numerical model

The wetness of a bidimensional foam is characterized by the area fraction of gas Φ. For $\Phi > 0.86$, the foam exhibits a finite yield stress. Here we focus on the limit of dry foams $\Phi \sim 1$. In this regime, the foam is composed of polygonal bubbles separated by thin liquid films (Weaire & Hutzler 1999). Three films intersect in regions called vertices, where most of the water is present (see figure 1*a*). Plasticity in two-dimensional dry foams arises through rapid local neighbour-switching events called $T1$ processes (figure 1*a*, *b*).

Several models have been developed to describe the flow behaviour of two-dimensional dry foams at finite shear-rate (Q-Potts models (Jiang *et al.* 1999); vertex model (Okuzono *et al.* 1993; Okuzono & Kawasaki 1995). The quasi-static algorithms (Weaire & Kermode 1983; Herdtle & Aref 1992; Weaire & Hutzler 1999), based on

the time-scale separation between the short duration of the plastic events τ_{T1} and the long characteristic time of shearing, provide a realistic description of the dynamics.

When the time scale associated with the imposed strain is large compared to the rearrangement time, the foam is at any time mechanically equilibrated (except during the rapid rearrangements). The foam structure minimizes the static free energy of the foam: for incompressible bubbles, this energy is proportional to the total film length. (The state equation of the gas is *a priori* necessary. However, for millimetric bubbles and typical surface tensions, the resulting relative changes in volume are negligible and the bubbles can be assumed incompressible.) Vertices have a typical size d_v set by the amount of water in the foam (figure 1). When the distance between two vertices is close to d_v, the foam becomes unstable and bubbles rearrange (T1 event, see figure 1*a*, *b*). The quasi-static shear simulation developed here is based on these arguments, and involves a loop over three main steps: (i) Compute the geometrical foam structure for the current bubble arrangement (the neighbouring relation between bubbles): the total film length is minimized under prescribed boundary conditions (described later) and a constraint of constant bubble area. (ii) The stability of the resulting structure with respect to topological rearrangements is then tested: if a film length falls below a threshold value (chosen to correspond to a gas fraction $\Phi = 0.99$), we modify the foam topology to account for the T1 event triggered (as in figure 1*a*, *b*). The minimal line-length structure is then recalculated. Steps (i) and (ii) are repeated until the structure is stable with regard to plastic events. (iii) A small increment of deformation is then applied, and the whole process of relaxation is started again. It should be stressed that this quasi-static model does not involve any description of the fast energy dissipation during the T1 process. This is correct as long as T1 events are well separated in time. It might, however, inaccurately describe situations where large avalanches occur (Weaire & Hutzler 1999). In this study, processes such as coarsening, coalescence or drainage are not taken into account.

The initial foam is created from the Voronoi tessellation of a disordered set of points (Weaire & Hutzler 1999), obtained by superimposing a Gaussian random displacement to an hexagonal lattice. The noise amplitude is used to tune the distribution of the resulting bubble areas. In this paper, the dimensions of the foams are $L_x \times L_y = 1.5 \times 1$, the system is periodic along the x-direction (see figure 1*c*). The upper and lower boundaries of the tessellation define the rigid walls. Their rough shape is preserved during the whole simulation. In this study, around 400 bubbles are packed between the two parallel walls. Their area distribution is presented in figure 1(*d*). In our unit system, the mean area and the standard deviation are, respectively, around 4×10^{-3} and 1×10^{-3}.

The energy minimization consists in the determination of the vertices positions and film curvatures which correspond to a minimum of the total line length. To reach this configuration, we use Surface Evolver (SE) Brakke (1992), a minimization software which has proved to be reliable for the computation of foam structures (Reinelt & Kraynik 2000; Kraynik, Reinelt & van Swol 2003). The conjugate gradient algorithm of SE rapidly ensures a locally equilibrated structure by computing the forces on each vertex and projecting the resulting trajectories along constraints (constant volume here). However, for extended networks, a large number of iterations is required in order to relax the soft modes of deformations associated with large- length-scale deformation fields. To bypass this limitation, the minimization process is separated into two distinct steps. (i) The foam structure is first reduced to a set of vertices connected by straight lines. The energy landscape associated with the structure is probed by imposing large-length-scale incompressible deformation fields, such as

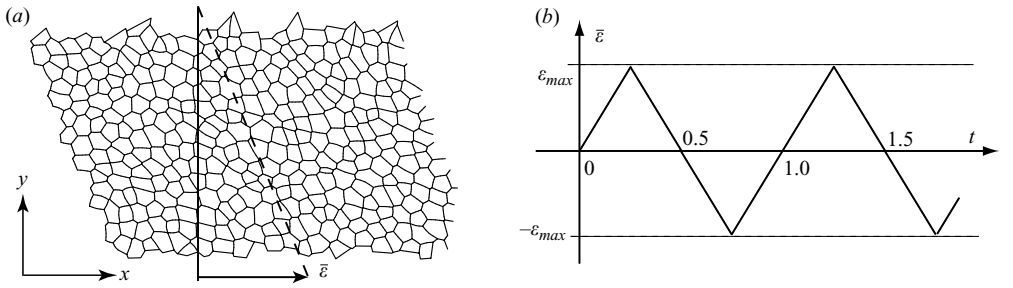

FIGURE 2. (*a*) A foam sample (16×24 bubbles) submitted to an imposed strain of amplitude $\bar{\varepsilon}$. (*b*) The oscillating strain sequence imposed to the foam in a typical experiment: t is the number of cycles and ε_{max} is the maximum strain amplitude. Movies corresponding to these simulations are available with the online version of the paper.

elementary shear or local rotation. When one of these strain fields decreases the total line-length energy, the associated displacement of the vertices is implemented. Details of this method are provided in the Appendix. (ii) When this minimization process has converged, the structure is progressively refined by adding degrees of freedom along the edges (up to eight points per edge). The energy minimization leads then to a structure satisfying the Plateau rules, which imply that three films meet at 120°. All the different physical quantities studied in this paper are measured on this final structure. This method allows us to study minute global deformation such as those observed in experiments (Debrégeas *et al.* 2001).

Shearing is imposed by progressively moving the lower wall from left to right, by small shear strain increments of 0.5 %. (This number ensures that each strain increment will trigger by itself at most one T1 event, although this first event might trigger further ones.) As expected in the quasi-static regime, moving the lower wall is strictly equivalent to moving the upper wall in the opposite direction. Hereinafter, lengths are scaled by the width L_y of the shearing gap, so that the displacement d of the lower wall is also the mean strain $\bar{\varepsilon} = d/L_y$. It should be noted that $\bar{\varepsilon}$ is the only control parameter for this study.

3. Quasi-static rheology

In this study, the foam is submitted to a shear strain oscillating between two symmetrical limits ε_{max} and $-\varepsilon_{max}$. As physical time is irrelevant in the quasi-static regime, any monotonic trajectory can be used to move the walls from one limit to the other. Along the lines of earlier similar studies (Weaire & Kermode 1983), we simply used, without a loss of generality, piecewise linear displacements of the walls. The evolutions of different structural and mechanical parameters are monitored as a function of the fractional number of applied cycles t (figure 2).

3.1. *Stress–strain relationship*

The coarse-grained shear stress over any subregion $\mathscr{D}$ of the sample can be extracted from the structure of the foam by using the following equation (Kraynik *et al.* 2003):

$$\sigma_{xy}(\mathscr{D}) = \frac{\gamma}{A(\mathscr{D})} \sum_{films\ i} \frac{l_{i,x} \cdot l_{i,y}}{l_i}. \tag{3.1}$$

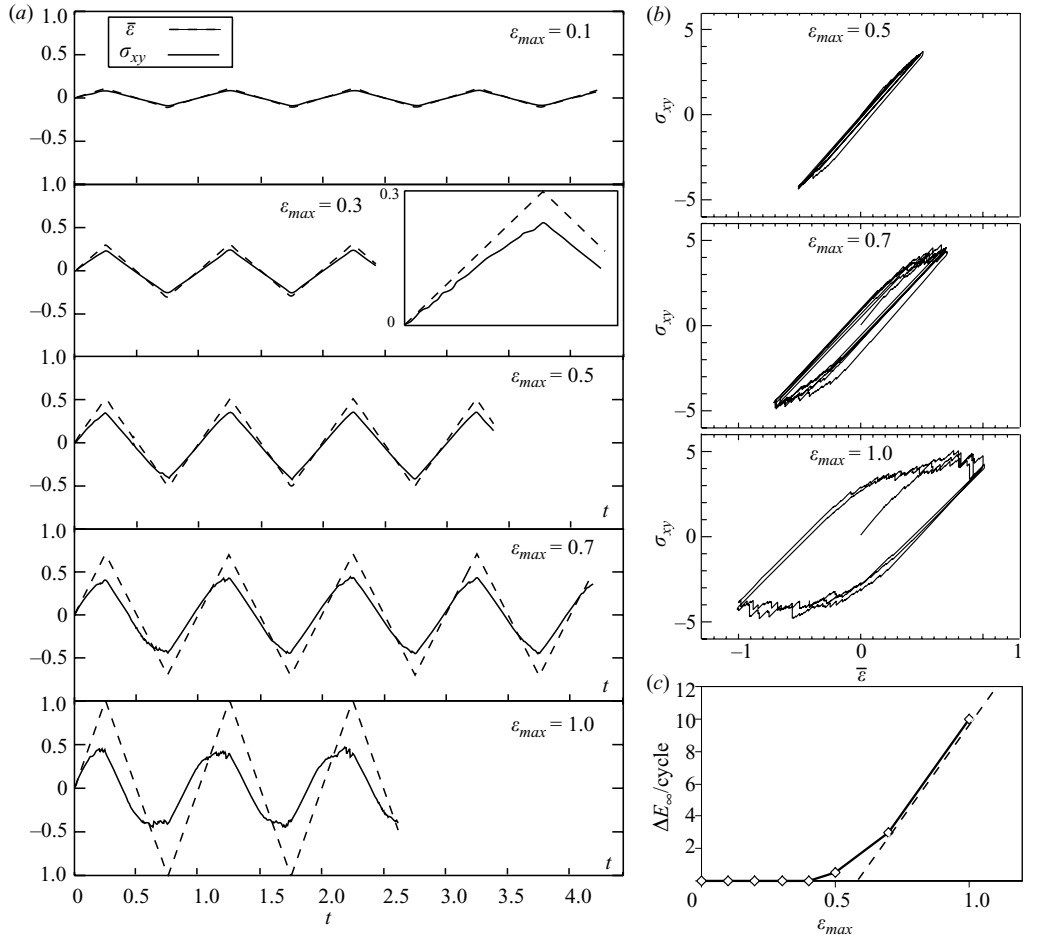

FIGURE 3. (*a*) Imposed strain (dashed lines) and shear stress (solid lines) as a function of t for different strain amplitudes $\bar{\varepsilon}_{max}$ (a magnification of 0.1 has been imposed to the stress measurements for clarity). The inset is a zoom of the first charge for $\bar{\varepsilon}_{max} = 0.3$. (*b*) Hysteresis cycles for different amplitudes. When $\bar{\varepsilon}_{max} < 0.5$, the behaviour becomes purely elastic after a transient of one or two cycles. (*c*) Energy dissipated per cycle in the permanent regime as a function of the shear strain amplitude.

The sum is performed over all the films lying within the subregion $\mathscr{D}$ of area $A(\mathscr{D})$. l_i is the length of the film, $l_{i,x}$ and $l_{i,y}$ are the projected lengths over the horizontal and vertical axis, respectively. Hereinafter, the line tension γ of the liquid film is set to 1.

By performing this calculation over the entire sample, the evolution of the total shear stress $\overline{\sigma_{xy}}$ exerted by the moving walls can be monitored. This quantity is shown in figure 3(*a*) as a function of the number of cycles t for different values of $\bar{\varepsilon}_{max}$ (dashed lines indicate the imposed strain). These graphs illustrate the elasto-plastic behaviour of foams under quasi-static shear: under low strain, the stress–strain relationship is linear. For imposed strain $\varepsilon_{max} \geqslant 0.5$, the stress reaches a yield value σ_Y. However, careful examination of the graphs reveals the occurrence of plastic events for stress values lower than the yield stress, especially during the first charge (inset in figure 3*a*).

3.2. *Transient, limit cycles and hysteresis*

Figure 3 shows the evolution of the shear stress with respect to the imposed strain, for different strain amplitudes. Consistently with the three-dimensional experimental measurements of Rouyer *et al.* (2003), the mechanical response of the foam is modified by the first cycles of deformation (shear ageing). After a few oscillations, a limit cycle is reached beyond which no apparent evolution of those properties can be detected. For a maximum strain $\overline{\varepsilon}_{max} < 0.5$, no more T1 events occur after one or two cycles. For $\overline{\varepsilon}_{max} \geqslant 0.5$, some irreversibility persists (figure 3*b*) and the associated dissipated energy can be measured by computing the area of the hysteresis loops in the limit cycle:

$$\Delta E_\infty = A \oint_{\text{limit cycle}} \sigma_{xy}(\varepsilon)\, \mathrm{d}\varepsilon, \tag{3.2}$$

where $A = L_x L_y$ denotes the total foam area. Figure 3(*c*) shows the evolution of this quantity for various strain amplitudes. As expected, ΔE_∞ is strictly zero for small amplitude. In the large-amplitude limit ($\varepsilon_{max} > 0.5$), the dissipation monotonously increases with ε_{max}, and ΔE_∞ can be described in that regime as an affine function of the imposed strain, corresponding to the area of the hysteresis cycles:

$$\Delta E_\infty = 4\ A\ \sigma_Y\ (\varepsilon_{max} - \overline{\varepsilon}_Y). \tag{3.3}$$

This allows us to identify a yield strain ε_Y as the maximum strain that the foam can sustain elastically. Beyond the yield strain, the foam flows under a well-defined shear stress, corresponding to the foam yield stress σ_Y (Khan *et al.* 1988). It should be noted, however, that these quantities are not intrinsic to the material: they may depend on the specific structure (the particular arrangement of the bubbles) of the foam, as well as its dimension.

In standard rheological measurements, this nonlinearity is expected to show up as a dependence of the complex shear modulus $G = G' + \mathrm{i}G''$ with the strain amplitude at vanishingly small shear rates (Rouyer *et al.* 2005 and references therein). Considering that the energy dissipated per cycle can be written as $\Delta E \approx G''\varepsilon_{max}^2$, we expect the loss modulus to depend on the strain amplitude as:

$$G'' \propto \sigma_Y \frac{\varepsilon_{max} - \varepsilon_Y}{\varepsilon_{max}^2}, \tag{3.4}$$

for strain amplitudes larger than the yield strain ε_Y; G'' should be null otherwise. This relation appears to be in good agreement with Rouyer *et al.* (2005) for imposed shear strain larger than the yield strain. For lower strain, the dissipation is dominated by coarsening-induced T1 events (Weaire & Hutzler 1999), which is not included in our model: this regime has been investigated numerically by Vincent-Bonnieu *et at*. (2006).

3.3. *Development of normal stress difference*

Development of normal stress difference upon shearing is commonly observed in a broad range of systems, from hyperelastic materials to complex fluids such as polymer solutions; it is in particular a characteristic feature of foams rheology (Khan & Armstrong 1986; Reinelt 1993; Reinelt & Kraynik 1996; Larson 1997; Hohler, Cohen-Addad & Labiausse 2004). In this section, we analyse the effect of shear-induced plasticity on normal stress difference, and focus on the regime of large applied strain ($\varepsilon_{max} = 1$). Figure 4 shows the first normal stress difference $\sigma_{xx} - \sigma_{yy}$ as a function of the number of cycles t and of the shear stress σ_{xy}. These graphs illustrate the strong coupling between these two quantities: the normal stress difference can

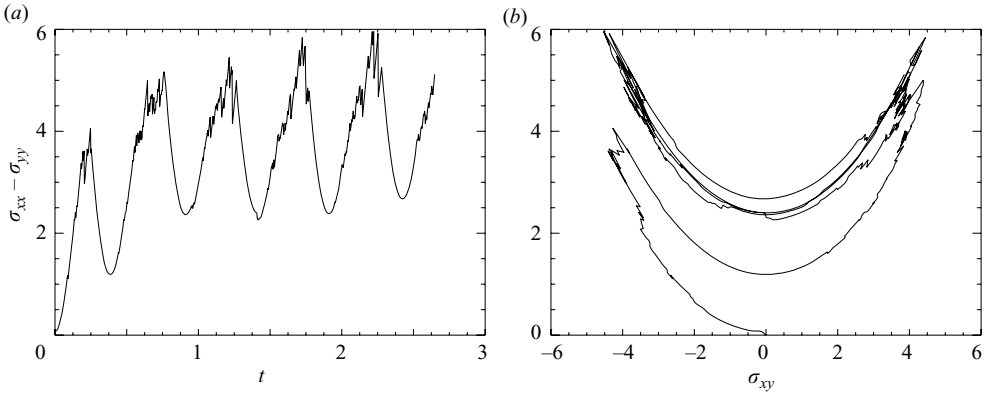

FIGURE 4. First normal stress difference as a function of (*a*) the number of shear cycles and (*b*) the shear stress. The maximum strain amplitude is $\varepsilon_{max} = 1$.

.

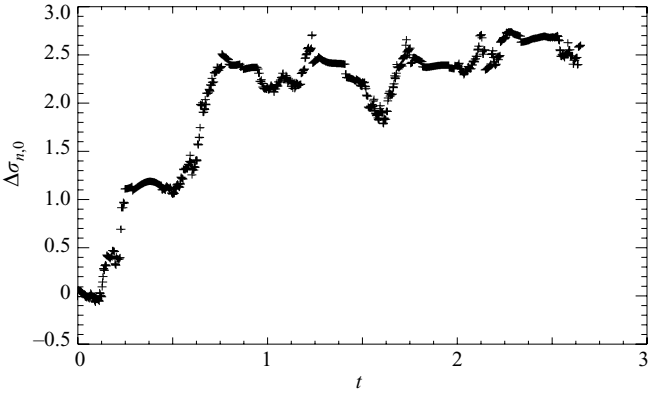

FIGURE 5. Normal stress difference under zero shear stress $\Delta\sigma_{n,0}$ as a function of the number of cycles t (maximum strain amplitude $\varepsilon_{max} = 1$).

be empirically described as a quadratic function of σ_{xy} with an offset $\Delta\sigma_{n,0}$ being a function of the number of cycles t:

$$\sigma_{xx} - \sigma_{yy} = \Delta\sigma_{n,0}(t) + \beta\sigma_{xy}^2. \tag{3.5}$$

The quadratic term is expected from the elastic deformation of the film network (Khan & Armstrong 1986), as will be detailed in the next section. In contrast, the offset corresponds to a permanent imprint in the material. To quantify the latter, the normal stress difference under zero shear stress $\Delta\sigma_{n,0}$ is evaluated by extrapolating the parabolic sections of the graphs of figure 4. As shown in figure 5, this quantity, plotted as a function of the number of applied strain cycles, exhibits (sample dependent) fluctuations about a slow global increase. This global increase cannot be explained by the elastic response, even with the nonlinear correction, as it occurs under zero shear stress. It is a signature of the structural evolution experienced by the foam under shear. This ability of foams to develop permanent normal stress difference is at the origin of the spatial heterogeneities of this mechanical quantity observed in real two-dimensional foams by Janiaud & Graner (2005).

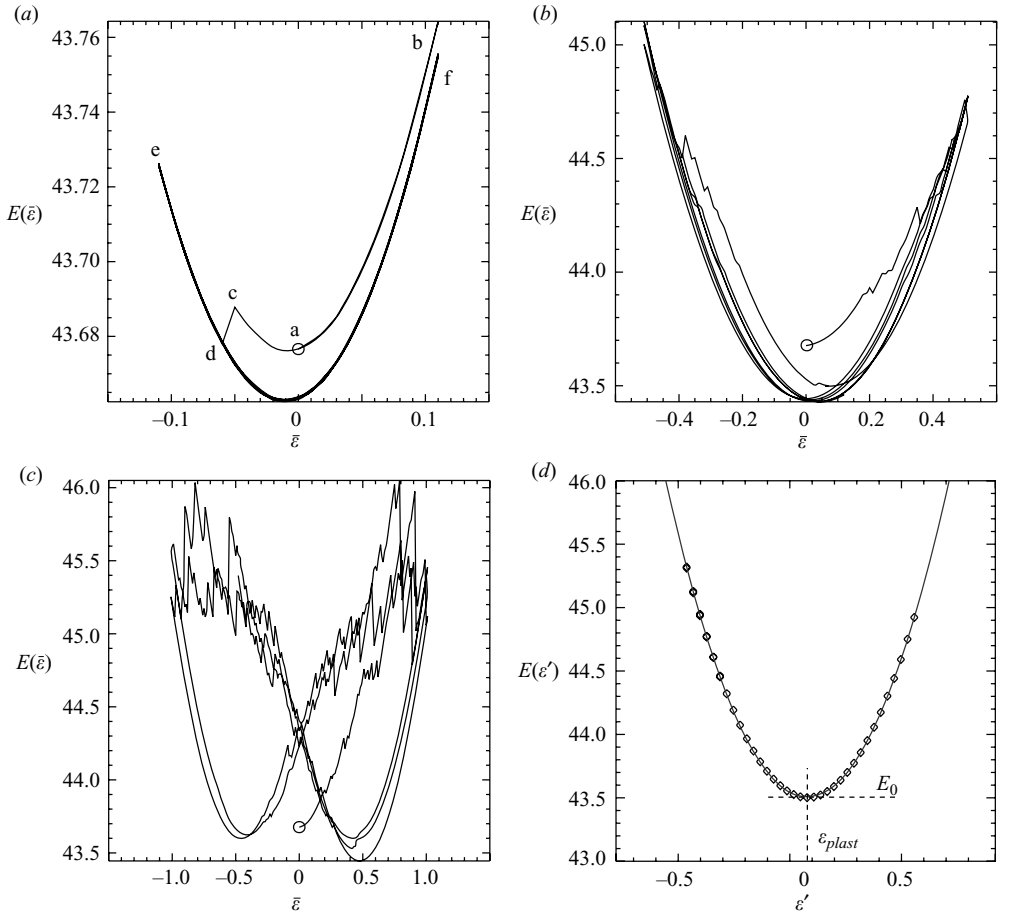

FIGURE 6. (*a–c*) Free energy of the foam as a function of the imposed strain, for three different amplitudes $\varepsilon_{max} = 0.1$, 0.5 and 1.0. The circles indicate the initial state, and the number of applied cycles is 3. The chronological trajectory in (*a*) is [a,b,a,c,d,e,d,f,d,e,d,f, ...] (*d*) Quadratic elastic basin associated with a given structure (see text). Symbols are numerical measurements, and the curve corresponds to the best parabolic fit.

3.4. *Energetic approach*

In order to further investigate the modification of the structural properties of the system under shear, we consider the evolution of the foam free energy (total line-length) with the imposed strain $\overline{\varepsilon}$ (figure 6). For the lowest strain amplitude, $\varepsilon_{max} = 0.1$, no rearrangement occurs during the first cycle of charge and discharge. The strain is reversible and the stress is a linear function of the strain. The following charge in the opposite direction generates one T1 event which induces a transition to a different energy basin.

The evolution of the system under shear can thus be seen as a series of transitions, induced by discrete plastic events, in a multistable potential landscape. Each configuration is associated with an elastic basin whose properties can be accessed by a quadratic extrapolation of the local energy versus deformation curve. The extrapolation must be performed in the elastic domain of response, in which no rearrangement takes place, and thus becomes increasingly inaccurate when the

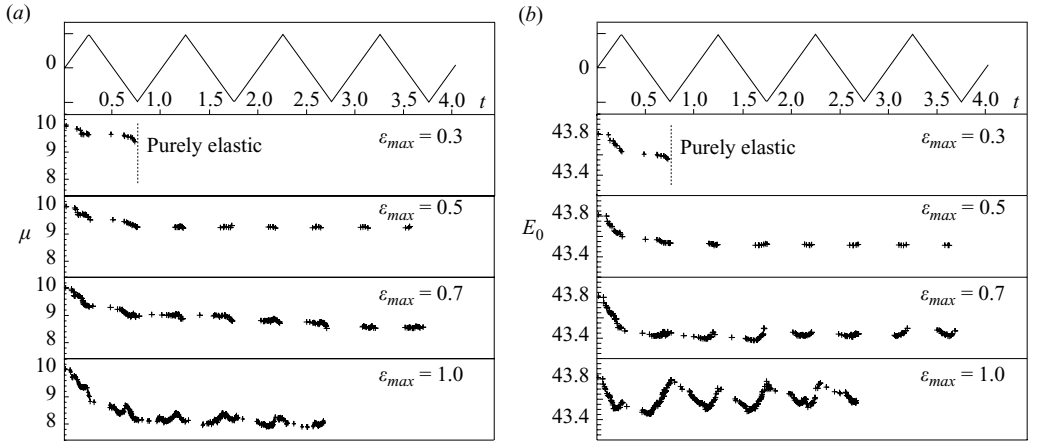

FIGURE 7. Evolution of (*a*) the shear modulus μ and of (*b*) the structural energy E_0 with the number of applied cycles t for different strain amplitudes (the top graphs show the associated imposed strain sequence). These quantities are evaluated after each T1 event and plotted at the instant of the rearrangement. For the lowest strain amplitude, no rearrangement occurs after the first cycle. The experiment was run for 3 cycles instead of 4 for the largest strain amplitude.

applied strain approaches the yield strain limit (figure 6*b*, *c*). To bypass this limitation, a specific numerical procedure is implemented: for every structure successively reached, a complete shear cycle of amplitude 0.5 is performed in which topological changes are forbidden. This numerical procedure allows us to produce an extended elastic basin, as shown in figure 6(*d*), on which an accurate quadratic fit can be performed:

$$E(\varepsilon') = E_0 + \tfrac{1}{2} A\mu\, (\varepsilon' - \varepsilon_{plast})^2, \tag{3.6}$$

where A is the foam area, μ is the shear modulus and E_0 is the minimal value of the energy reached under zero shear stress. These two latter quantities are specific to the structure and do not depend on the elastically stored shear deformation. It should be noted that E_0 cannot be extracted from mechanical measurements which only depend on the derivative of the potential. Hereinafter, E_0 will be referred to as the structural energy of the foam. The quantity ε_{plast} corresponds to the applied strain (or to the position of the lower wall) for which the foam energy is minimum and the shear stress is 0.

Figure 7 shows the evolution of the shear modulus μ and of the structural energy E_0 as the foam undergoes successive strain oscillations. A systematic decrease of μ is observed with the number of cycles, this effect being stronger for increasing strain amplitude. This observation is consistent with the experimental rheological measurements made on three-dimensional foam by Hohler, Cohen-Addad & Asnacios, (1999). The same behaviour is observed for E_0 which indicates the existence of a strain-induced structural relaxation process. For large shear amplitude, however ($\varepsilon_{max} > 0.7$), the value of the structural energy exhibits oscillations: its value reaches a maximum whenever the absolute value of the applied strain is maximum. This behaviour is associated with the development of heterogeneities in the spatial distribution of the T1 events, as will be shown later in the paper.

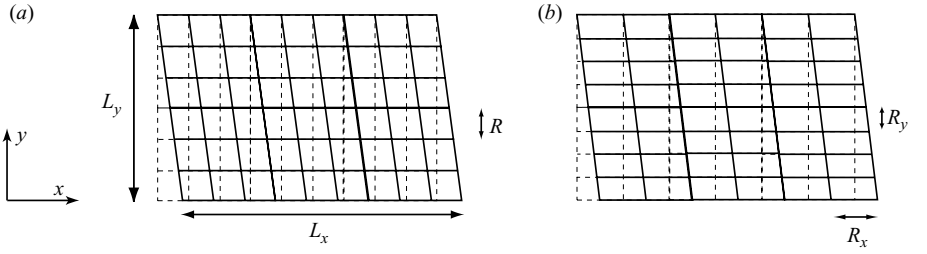

FIGURE 8. Simplified foam models: (*a*) isotropic: a square films network is sheared along the *x*-axis (the dashed grid represents the unsheared configuration), (*b*) anisotropic: the foam consists of rectangular cells which deform into parallelograms as the system is sheared.

4. Interpretation

The structural evolution of the foam under moderate shearing ($\varepsilon_{max} < 0.7$) is associated with (i) the appearance of normal stress difference, (ii) a structural energy relaxation, (iii) a decrease of the shear modulus. These evolutions result from the strain-induced topological rearrangements that irreversibly modify the foam structure. In this section, we attempt to account for these observations by first examining the effect of the film network anisotropy on both the normal stress difference and the shear modulus, using a simplified foam model. We then focus on the evolution of topological disorder to interpret the decrease in the structural energy.

4.1. *Shear modulus and normal stress difference*

As first recognized by Princen (1983), the main characteristics of foam elasticity can be understood by considering the film elongation induced by the deformation of a regular network of liquid films.In order to relate the slow increase of the normal stress difference under zero shear stress to the softening of the foam, we use in this section a minimal model based on Alexander's (1998) square foam model. We consider a square network of films with dimension $L_x \times L_y$, and surface tension γ. R denotes the distance between adjacent films in the original (undeformed) structure (figure 8*a*). This simplified model only focuses on the elastic behaviour due to film elongation and reorientation upon shear, and ignores disorder as well as Plateau's rule which imposes films to meet at an angle of 120°. When the network is strained along the horizontal *x*-direction, the length of the horizontal films remains unchanged, whereas the length of the vertical films varies with the shear strain ε_{xy} by a quantity:

$$\delta l(x) = L_y\sqrt{1+\varepsilon_{xy}^2} - L_y. \tag{4.1}$$

Assuming that each film acts on the structure with a force of intensity γ, simple geometry allows us to write the different components of the stress tensor to second order in the applied deformation ε_{xy}:

$$\sigma_{xy} = \mu_0\varepsilon_{xy}, \tag{4.2}$$

$$\sigma_{xx} = \frac{\gamma}{R}\left(1+\varepsilon_{xy}^2\right) = \mu_0\left(1+\varepsilon_{xy}^2\right), \tag{4.3}$$

$$\sigma_{yy} = \frac{\gamma}{R}\left(1-\tfrac{1}{2}\,\varepsilon_{xy}^2\right) = \mu_0\left(1-\tfrac{1}{2}\,\varepsilon_{xy}^2\right), \tag{4.4}$$

where $\mu_0 = \gamma/R$ is the shear modulus (a better estimate is obtained with a hexagonal network that takes into account the local equilibrium rule of the liquid films (Princen 1983)). Consisitently with Khan & Armstrong (1986), the quadratic relationship

between the shear stress and the normal stress difference immediately follows:

$$\sigma_{xx} - \sigma_{yy} = \frac{3}{2}\frac{\gamma}{R}\varepsilon_{xy}^2 = \frac{3}{2}\frac{\sigma_{xy}^2}{\mu_0}. \tag{4.5}$$

We observed in the previous section the appearance of a finite normal stress difference under zero shear stress. This indicates that an oscillating strain induces a relative increase of the average density of films in the shear direction in comparison to the normal direction. In order to illustrate this effect, we introduce anisotropy in the previous model (figure 8*b*) by considering a film network made of parallelograms of area $R_x \times R_y$. The equivalent cell size is defined as $R = \sqrt{R_x \times R_y}$ and the structure anisotropy is characterized by two geometrical parameters:

$$a_{xx} = R_x/R - 1, \quad a_{yy} = R_y/R - 1. \tag{4.6}$$

The anisotropy is therefore associated with a pre-strain of the material along the shear axis. As for the square lattice, we evaluate the mechanical properties of the foam. The line-length energy is:

$$E(\varepsilon_{xy}) = E_0 + \tfrac{1}{2}A\frac{\gamma}{R}(1 - a_{xx})\varepsilon_{xy}^2, \tag{4.7}$$

with

$$E_0 = \frac{2\gamma A}{R}\left(1 + \tfrac{1}{2}a_{xx}^2 + \tfrac{1}{2}a_{yy}^2\right). \tag{4.8}$$

The tangent shear modulus is thus:

$$\mu = \frac{1}{A}\frac{\partial E}{\partial \varepsilon_{xy}} = \frac{\gamma}{R}(1 - a_{xx}). \tag{4.9}$$

The previous relations show that the anisotropy, or prestrain, affects both the structural energy E_0 and the tangent shear modulus μ. It should be noted that the modulus μ only applies to shear along the x-direction. This simple model provides a prediction for the normal stress components as a function of the shear strain ε_{xy} and the anisotropy defined by a_{xx} and a_{yy}:

$$\sigma_{xx} = \frac{\gamma}{R}(1 - a_{yy}) + \frac{\gamma}{R}(1 - a_{xx})\varepsilon_{xy}^2, \tag{4.10}$$

$$\sigma_{yy} = \frac{\gamma}{R}(1 - a_{xx}) - \frac{\gamma}{2R}(1 - a_{xx})\varepsilon_{xy}^2. \tag{4.11}$$

To first order in ε_{xx}, the area conservation ($R_x R_y = R^2$) imposes that $a_{xx} + a_{yy} = 0$, so that the normal stress difference under zero shear stress reads:

$$\sigma_{xx} - \sigma_{yy} = \underbrace{\frac{\gamma}{R}(2a_{xx})}_{\Delta\sigma_{n,0}} + \frac{3}{2}\frac{\gamma}{R}(1 - a_{xx})\varepsilon_{xy}^2. \tag{4.12}$$

By substituting this expression into (4.9), we can derive a relationship between the normal stress difference under zero shear stress $\Delta\sigma_{n,0}$ and the shear modulus:

$$\mu = \mu_0 - \tfrac{1}{2}\Delta\sigma_{n,0}, \tag{4.13}$$

where $\mu_0 = \gamma/R$ is the shear modulus of the equivalent isotropic foam.

This relation suggests testing the correlation between these two quantities measured in the numerical simulation. The expected proportionality is observed in spite of the fluctuations of these two parameters (figure 9). It should be noted, however, that the

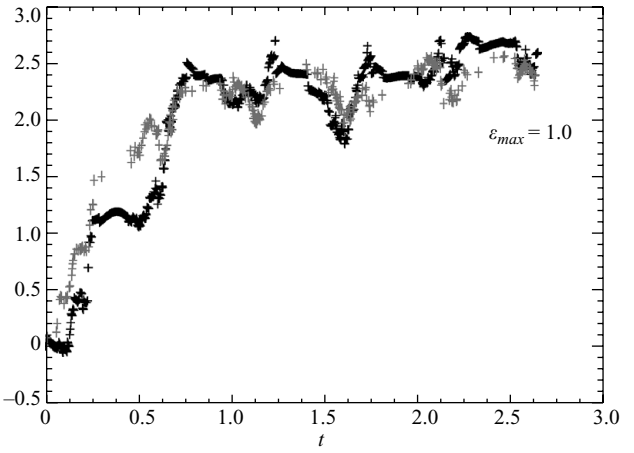

FIGURE 9. Normal stress difference under zero stress $\Delta\sigma_{n,0}$ (black) and variation of the shear modulus $\mu_0 - \mu$ (grey) as a function of the number of cycles t, extracted from the numerical simulation with a strain amplitude $\varepsilon_{max} = 1$. The shear modulus variations have been multiplied by 1.25 to underline the similar evolution of both quantities.

ratio $(\mu_0 - \mu)/\Delta\sigma_{n,0}$ is of the order of 0.8 in the numerical system instead of the expected 0.5 predicted by this model. This discrepancy can be accounted for by the simplicity of the model, which does not take into account either Plateau's rule or the polydispersity of the foam. Nevertheless, it illustrates that both quantities reflect the distribution of the film orientation with regard to the shearing direction. The strain-induced T1 processes tend to orientate the films in the direction of the shear, thus driving the structure into an anisotropic state.

4.2. *Relaxation of the disorder and transition to the plastic flow*

The anisotropic model presented above yields an expression of E_0 as a function of the geometrical parameters a_{xx} and a_{yy} (equation (4.8)): this corresponds to the energy associated with the pre-strain built in by the plastic events. Based on this expression, we would expect E_0 to increase with the imposed maximum strain, in contradiction with our observations. This model, however, ignores the foam disorder, which can influence E_0 and might evolve upon shearing.

One standard way to evaluate topological disorder in dry foams consists in measuring the second moment μ_2 of the distribution $P(n)$ of the number of films per bubble (Weaire & Hutzler 1999). In two-dimensional dry foams, the average number of neighbours per bubble is exactly 6, which yields the following expression for μ_2:

$$\mu_2 = \sum_n (n-6)^2 P(n). \tag{4.14}$$

In agreement with previous experimental (Abd el Kader & Earnshaw 1999) and numerical (Kraynik *et al.* 2003) studies, moderate shearing produces a partial relaxation of the topological disorder (figure 10). By curing topological defects originally present in the foam, the shearing extends the elastic domain. This shear-strengthening process has its counterpart in other systems such as dense colloidal glasses or friction joints (Bureau *et al.* 2002; Viasnoff & Lequeux 2002; Baumberger & Caroli 2006). Although the decrease of E_0 under low strain can be accounted for by this topological relaxation, the oscillations of E_0 at larger deformation remain unexplained. Neither

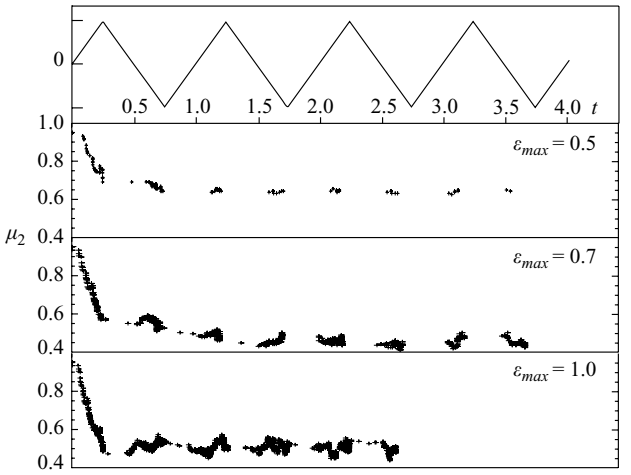

FIGURE 10. Evolution of the topological disorder. The second moment μ_2 of the distribution of the number of films per bubble is plotted as a function of the number of applied cycles t for different strain amplitudes ε_{max}. The top graph shows the associated imposed strain sequence.

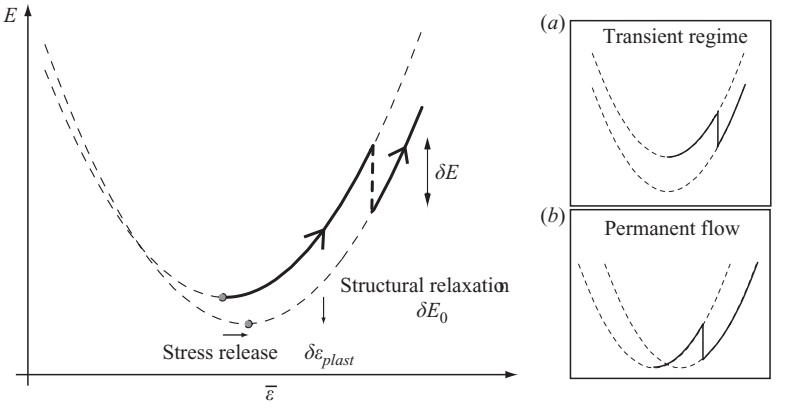

FIGURE 11. Shift of the elastic basin following a T1 event. Two main mechanisms can be distinguished: (*a*) relaxation of the structural disorder (mostly during transient regime), and (*b*) relaxation of the imposed shear stress.

the anisotropy (measured by the normal stress difference under zero shear stress) nor the topological disorder (measured by μ_2) exhibit a similar behaviour.

In order to understand this process, we must look in more detail at the effect of T1 events on the energy basin of the foam. When a rearrangement T1 occurs during the shearing, a certain amount of energy δE is relaxed (figure 6). δE is found to be systematically of order $-\gamma D$, where D is the mean bubble diameter. This energy release may be decomposed into two terms (figure 11):

$$\delta E = \delta E_0 - A\, \sigma_{xy}\, \delta\varepsilon_{plast}. \tag{4.15}$$

The first term is associated with a relaxation of the structural energy E_0. The second term corresponds to a partial relaxation of the applied shear stress σ_{xy}, which induces a lateral shift in the position of the minimum of the energy basin. The relative value of the structural and shear stress relaxation strongly depends on the system preparation.

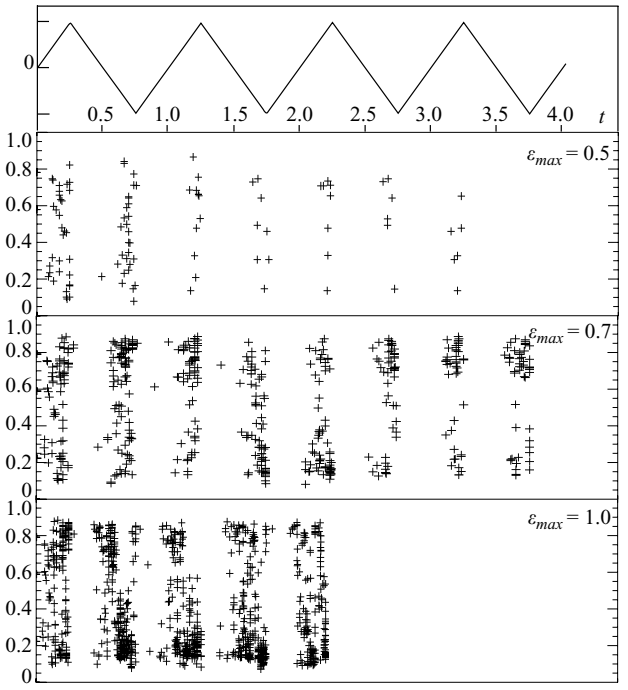

FIGURE 12. Positions of the T1 rearrangements across the gap during the shearing, for different amplitudes ε_{max}. For each T1 event, occurring at the instant t, a cross is placed whose ordinate corresponds to its distance to the lower wall.

Figures 6 and 7(*b*) show that, under low deformation ($\varepsilon_{max} \leqslant 0.5$), T1 events mainly relax the structure. At higher imposed strain, the main effect of the rearrangements is a relaxation of the applied shear stress. When the shear stress becomes high, δE_0 (equation (4.15)) can be positive, leading to the increase of E_0 observed in figure 7(*b*): the stress release occurs at the expense of the structure relaxation. The oscillations of the structural energy may therefore be understood as a series of shear stress relaxations (which increase the structural heterogeneities) and disorder relaxations when the shear stress is reversed.

The transition to plastic flow can also be studied by looking at the spatial distribution of the rearrangements during shearing (figure 12). For low strain amplitude $\varepsilon_{max} \leqslant 0.5$, T1 events are uniformly distributed inside the foam. For higher amplitude in contrast, they occur preferentially in the vicinity of the walls. These observations reflect the fact that transient T1 events arise from the relaxation of the homogeneous initial disorder, whereas plastic events occurring at larger length scales have a more complex dependence on the system geometry and history. This is, moreover, consistent with the appearance of a shear band observed under continuous slow shear in a similar geometry (Kabla & Debrégeas 2003).

5. Conclusion

The response of a two-dimensional foam to an oscillating quasi-static shear exhibits a transient regime: during the first few shear cycles, various mechanical properties evolve with time as a result of the shear-induced plastic events.

For moderate strain amplitude ($\varepsilon_{max} \leqslant 0.5$), the elastic modulus is found to decrease, and a finite normal stress difference at zero shear stress develops. This evolution is a consequence of the building up of anisotropy in the film network. The plastic events reduce the topological disorder as indicated by a decrease of the second moment μ_2 of the distribution of the number of films per bubble, and a reduction of the free energy E_0 of the foam at zero shear stress. This results in an enlargement of the elastic domain, i.e. the range of strain that the foam can sustain elastically.

At larger strain amplitude ($\varepsilon_{max} \geqslant 0.5$), a different behaviour is observed: as the number of plastic processes suddenly increases, they tend to relax the applied shear stress at the expense of the structural relaxation observed at low shear strain. As a consequence, the energy E_0 increases, and thus exhibits oscillation within a complete strain cycle. This process is associated with the development of spatial heterogeneities in the distributions of the T1 processes. Instead of being homogeneously distributed all across the gap, they tend to gather near the shearing wall. This elastic to plastic transition will be studied in detail in Part 2 where the fully developed flow regime is probed, both numerically and experimentally.

The present study shows how the evolution of structural properties can allow us to understand the shear-history dependence of disordered systems at zero temperature. It reveals that the applied shear stresses bias the plastic events selection in a non-trivial way, which leads to the two regimes of relaxation detailed in this paper. Further work will be required in order to understand this process precisely.

Appendix. Numerical procedure for the energy minimization

A.1. *Large-length-scale deformations*

Gradient methods, such as that used by Surface Evolver (SE) to minimize the foam energy, drive the system down the steepest slope of the energy landscape. After each iteration, geometrical constraints are taken into account by projecting the trajectory along specific directions. In the case of the SE algorithm, this allows us to ensure that each bubble area remains constant throughout the process. When a large number of constraints is imposed, it appears, however, that large-length-scale modes of deformation are very slowly relaxed by the standard conjugate gradient methods, leading to a lack of precision in the resulting structure.

In order to evaluate the efficiency of the minimization procedure, we impose large-length-scale deformations to a film network, and then allow for the energy to relax. We start with the initial structure shown in figures 13(*a*) and 13(*e*), obtained after a thousand iterations of SE. At this stage, the foam is simply made of straight edges, with a fixed volume constraint per bubble. We then impose two distinct modes of deformation: simple shear from the boundary (figure 13*b*) and large-length-scale torsion (figure 13*f*), which includes rotations and dilatations.

Figures 13(*c*) and 13(*g*) show the result of a few thousand iterations of the conjugate gradient method applied to the deformed structures (we note that for these tests, T1 events are not included in the minimization process). Although all cells then satisfy the constant volume constraint, the final configuration is still far from equilibrium: the imposed deformations are clearly visible in the resulting network. More iterations would lead to a better minimization, but the energy evolves extremely slowly.

In the case of a simple shear, it is usually valid to prescribe, prior to the minimization steps, a linear displacement field according to the wall position. It guarantees most of the time that each bubble would start close to its equilibrium position. However, in cases where the expected flow profile itself is debated, such a 'guess' must be

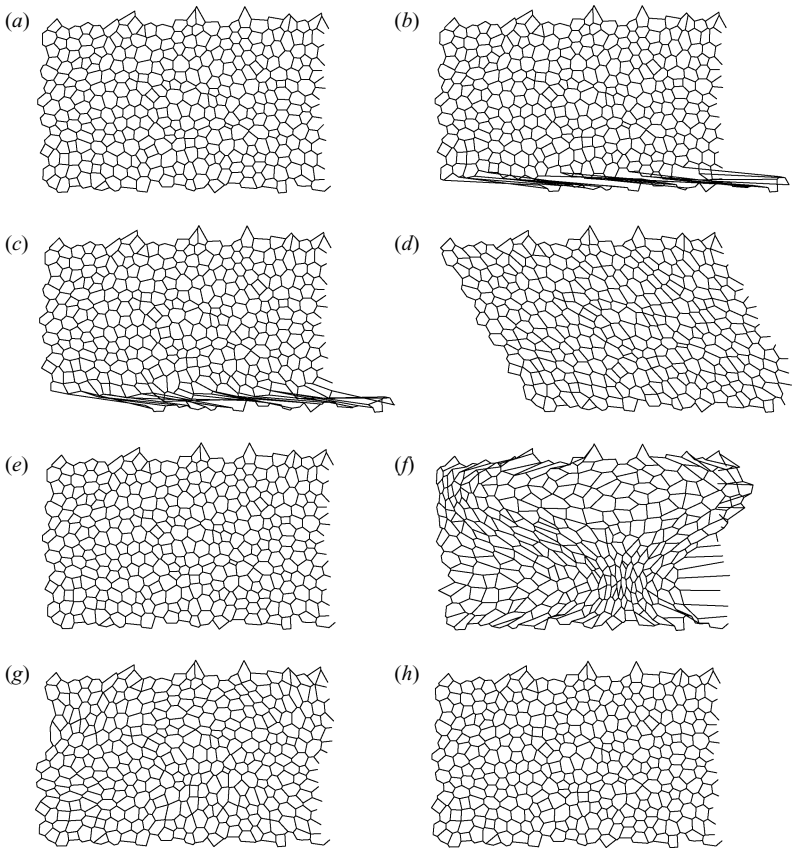

FIGURE 13. Tests of the energy minimization procedures. (*a–d*) Relaxation of a 30% shear induced by the boundary. (*a*) Initial configuration after 1000 CG step. (*b*) Unequilibrated structure after the wall is moved. (*c*) Relaxation profile obtained using CG iterations only. (*d*) Structure obtained by coupling the gradient descent with soft mode testing. (*e–h*) Relaxation of an internal distortion of the foam structure. (*e*) Initial configuration after 1000 CG step. (*f*) Unequilibrated structure after the wall is moved. (*g*) Relaxation profile obtained using CG iterations only. (*f*) Structure obtained by coupling the gradient descent with soft mode testing.

avoided since it may induce a bias on the resulting behaviour. Furthermore, it has been shown that a large part of the relaxation field in sheared foams is associated with large-length-scale rotating modes (Debrégeas *et al.* 2001). A realistic algorithm should therefore be able to correctly relax these soft elastic modes.

We must thus use purely energetical approaches to guarantee that, after an incremental shear deformation or a T1 event, the structure is entirely equilibrated over the system size.

A.2. *Elementary test deformations*

In order to achieve a proper minimization, we use (in addition to the conjugate gradient method) a Monte-Carlo type algorithm which tests series of random large-length-scale deformations. We implement two families of deformation fields, corresponding qualitatively to the kinds of deformation previously described: shear along the walls, and local rotation fields. These fields satisfy, at least in the limit of small deformation, the constraint of incompressibility of the material and the no-slip

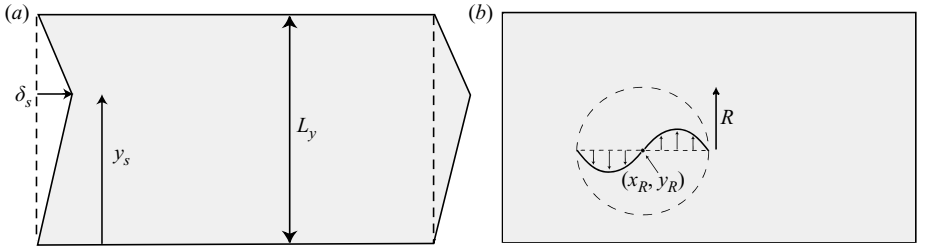

FIGURE 14. Elementary soft deformation modes used to approach the foam equilibrium configuration. (*a*) Shear test deformation, defined by the amplitude and orientation δ_s, and by the location y_s of the maximum displacement. (*b*) The roll test deformation is centred on (x_R, y_R). The roll diameter is R, and the angular direction and rotation amplitude is defined by δ_R.

boundary conditions. We show in § A.3 that any deformation field compatible with these constraints can be decomposed as a sum of such elementary deformations fields.

A.2.1. *Shear deformation*

The first family corresponds to displacement fields that can be written as:

$$\boldsymbol{u}_s(x, y) = \begin{cases} \delta_s \dfrac{y}{y_s} & \boldsymbol{u}_x \quad \text{for } y < y_s, \\ \delta_s \dfrac{L_y - y}{L_y - y_s} & \boldsymbol{u}_x \quad \text{for } y > y_s, \end{cases} \tag{A 1}$$

where y_s is an arbitrary position inside the foam ($0 < y_s < L_y$) and δ_s is the maximum displacement. Such a displacement field is sketched in figure 14(*a*). The minimization proceeds as follow: after a few iterations of the conjugate gradient method, we randomly pick a position y_s and a shear direction represented by the sign of δ_s. We then move the structure according to the corresponding displacement field $u_s(x, y)$ (equation (A 1)) with an amplitude δ_s of the order of a tenth of a bubble diameter. We apply a few SE iterations to adjust the structure at the bubble scale. If the resulting deformation lowers the total energy, the same field is applied again and the process is repeated as long as the energy keeps decreasing, otherwise, the same test deformation is applied with an opposite sign for δ_s. The process is repeated for other values of y_s, until no more significant energy reduction can be obtained through this method. This algorithm is able to relax the structure in figure 13(*b–d*) in a few seconds.

A.2.2. *Roll deformation*

A second type of test deformation is used, which corresponds to local rotations as illustrated in figure 14. The corresponding displacement field is:

$$\boldsymbol{u}_R(r, \theta) = \begin{cases} \delta_R \sin(\pi r/R) & \boldsymbol{u}_\theta \quad \text{for } r < R, \\ 0 & \boldsymbol{u}_\theta \quad \text{for } r > R. \end{cases} \tag{A 2}$$

The roll, of radius R, is centred in (x_R, y_R) and r is the distance from the centre. In the present case, the coordinates of the centre are randomly picked, then the radius is chosen in the interval $R \in [D_b, min(x_R, L_y - x_R)]$ where D_b is a cutoff distance below which the structure can be properly relaxed by conjugated gradient methods (typically 2 bubble diameters). We then follow the same algorithm as for the test shear deformations. A larger number of iterations are required to relax the structure since there are more parameters to vary. However, it achieves a satisfactory

minimization of the structure much faster than the conjugate method gradient alone would do. Figure 13(*h*) has been obtained with this process after a few minutes of iterations which should be compared to figure 13(*g*) obtained after a similar processing time.

A.3. *Residual deformation of an incompressible two-dimensional material*

The method described above dramatically reduces the minimization process time. However, in order to reach the true minimum energy configuration, the test fields introduced above should be able to account for any large-scale deformation of the foam structure, compatible with the boundary conditions and incompressibility constraints.

We define the two-dimensional field $\boldsymbol{u}(x, y) = (u_x(x, y), u_y(x, y))$ as the displacement field leading from the actual configuration to the unknown configuration of minimal energy. As Surface Evolver ensures the conservation of the bubble volume, this displacement field is incompressible ($\nabla \boldsymbol{u} = 0$). The field $\boldsymbol{u}$ therefore derives from a scalar field $\psi(x, y)$ such as:

$$u_x = \frac{\partial \psi(x, y)}{\partial y}, \tag{A 3}$$

$$u_y = -\frac{\partial \psi(x, y)}{\partial x}. \tag{A 4}$$

Since the foam is attached to the walls, located at $y = 0$ and $y = L_y$, the residual field is necessarily null along the walls ($u_x(x, 0) = u_y(x, 0) = 0$ and $u_x(x, L_y) = u_y(x, L_y) = 0$). This implies that the potential satisfies $\partial\psi/\partial x = \partial\psi/\partial y = 0$ along the rigid walls: the potential is constant at the vicinity of the boundaries. Such a function is sketched on figure 15(*a*).

In order to validate our algorithm further, we must show that any potential satisfying the previous condition can be decomposed into a sum of the potentials of the test fields previously introduced.

The integration of (A 3) for the field associated with the shear test deformation yields, for the potential ψ_s:

$$\psi_s = \frac{1}{2}\frac{\delta_L}{y_L} y^2 \text{ for } y < y_L, \tag{A 5}$$

$$\psi_s = -\frac{1}{2}\frac{\delta_L}{L_y - y_L}(L_y - y)^2 + \frac{1}{2}\delta_L L_y \text{ for } y > y_L. \tag{A 6}$$

This potential, whose typical shape is described in figure 15(*b*), satisfies (A 3). Having a residual shear in the system is associated with a potential difference $\psi(y = L_y) - \psi(y = 0)$ between the two walls. By applying a series of test shear deformations, the potential associated with the residual distortion can thus be made null at the boundaries (see figure 15*c*).

The second family of test deformations, defined by (A 2), leads to the following expression for the associated potential (expressed here in polar coordinates centred on the roll):

$$\psi_R = \frac{\delta_r R}{\pi}\left(\cos\left(\pi\frac{r}{R}\right) + 1\right) \text{ for } r < R, \tag{A 7}$$

$$\psi_R = 0 \text{ for } r > R, \tag{A 8}$$

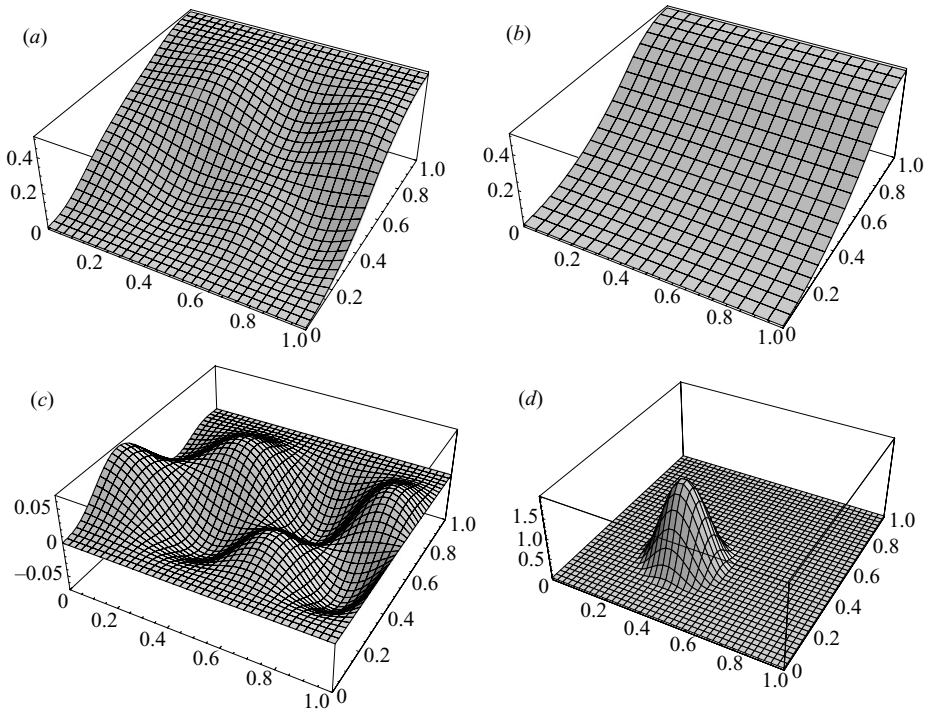

FIGURE 15. Examples of potentials associated with the deformation fields for (*a*) a typical residual deformation, (*b*) a shear along the wall direction $\psi_s(x, y)$ (for $y_L = 0.7$), (*c*) a typical residual deformation after the relaxation of the shear modes, (*d*) a roll deformation.

where R is the radius of the local roll. This corresponds to a family of bell-shaped functions with compact support; an example is shown in figure 15(*d*). It is easy to show that any potential whose value and derivative is null at the boundaries can be decomposed into a sum of such functions.

REFERENCES

ABD EL KADER, A. & EARNSHAW, J. C. 1999 Shear-induced changes in two-dimensional foam. *Phys. Rev. Lett.* **82**, 2610–2613.

ALEXANDER, S. 1998 Amorphous solids: their structure, lattice dynamics and elasticity. *Phys. Rep.* **296**, 65–236.

BAUMBERGER, T. & CAROLI, C. 2006 Solid friction from stick–slip to pinning and aging. *Adv. Phys.* **55**, 279–348.

BRAGG, L. & NYE, J. F. 1947 A dynamical model of a crystal structure. *Proc. R. Soc. Lond.* A **190**, 474–482.

BRAKKE, K. 1992 The surface evolver. *Expl Maths* **1**, 141–165.

BULATOV, V. V. & ARGON, A. S. 1994*a* A stochastic model for continuum elasto-plastic behavior: I. Numerical approach and strain localization. *Modelling Simul. Mater. Sci. Engng.* **2**, 167–184.

BULATOV, V. V. & ARGON, A. S. 1994*b* A stochastic model for continuum elasto-plastic behavior: II. A study of the glass transition and structural relaxation. *Modelling Simul. Mater. Sci. Engng* **2**, 185–202.

BULATOV, V. V. & ARGON, A. S. 1994*c* A stochastic model for continuum elasto-plastic behavior: III. Plasticity in ordered versus disordered solids. *Modelling Simul. Mater. Sci. Engng* **2**, 203–222.

BUREAU, L., BAUMBERGER, T. & CAROLI, C. 2002 Rheological aging and rejuvenation in solid friction contacts. *Eur. Phys. J. E* **8**, 331–337.

Cantat, I. & Delannay, R. 2005 Dissipative flows of 2D foams. *Eur. Phys. J.* E **18**, 55–67.

Debrégeas, G., Tabuteau, H. & di Meglio, J.-M. 2001 Deformation and flow of a two-dimensional foam under continuous shear. *Phys. Rev. Lett.* **87**, 178305.

Dennin, M. & Knobler, C. M. 1997 Experimental studies of bubble dynamics in a slowly driven monolayer foam. *Phys. Rev. Lett.* **78**, 2485–2488.

Derec, C., Ajdari, A. & Lequeux, F. 2001 Rheology and aging: a simple approach. *Eur. Phys. J.* E **4**, 355–361.

Dollet, B., Elias, F., Quilliet, C., Raufaste, C., Aubouy, M. & Graner, F. 2005 Two-dimensional flow of foam around an obstacle: force measurements. *Phys. Rev.* E **71**, 031403.

Falk, M. L. & Langer, J. S. 1998 Dynamics of viscoplastic deformation in amorphous solids *Phys. Rev.* E **57**, 7192.

Fisher, D. S., Fisher, M. P. A. & Huse, D. A. 1991 Thermal fluctuations, quenched disorder, phase transitions, and transport in type-II superconductors. *Phys. Rev.* B **43**, 130–159.

Herdtle, T. & Aref, H. 1992 Numerical experiments on two-dimensional foam. *J. Fluid Mech.* **241**, 233.

Hohler, R. & Cohen-Addad, S. 2005 Rheology of liquid foam. *J. Phys.: Condensed Matter* **17**, R1041–R1069.

Hohler, R., Cohen-Addad, S. & Asnacios, A. 1999 Rheological memory effect in aqueous foam. *Europhys. Lett.* **48**, 93–98.

Hohler, R., Cohen-Addad, S. & Labiausse, V. 2004 Constitutive equation to describe the non-linear elastic response of aqueous foams and concentrated emulsions. *J. Rheol.* **48**, 679–690.

Janiaud, E. & Graner, F. 2005 Foam in a two-dimensional Couette shear: a local measurement of bubble deformation. *J. Fluid Mech.* **532**, 243–267.

Janiaud, E., Weaire, D. & Hutzler, S. 2006 Two-dimensional foam rheology with viscous drag. *Phys. Rev. Lett.* **97**, 038302.

Jiang, Y., Swart, P. J., Saxena, A., Asipauskas, M. & Glazier, J. A. 1999 Hysteresis and avalanches in two-dimensional foam rheology simulations. *Phys. Rev.* E **59**, 5819.

Kabla, A. & Debrégeas, G. 2003 Local stress relaxation and shear-banding in a dry foam under shear. *Phys. Rev. Lett.* **90**, 258303.

Kabla, A, Scheibert, J. & Debrégeas, G. 2007 Quasi-static rheology of foams Part 2. Continuous shear flow. *J. Fluid Mech.* **587**, 45–72.

Khan, S. A. & Armstrong, R. C. 1986 Foam rheology: I Theory for dry foams. *J. Non. Newtonian Fluid Mech.* **22**, 1–22.

Khan, S. A., Schnepper, C. A. & Armstrong, R. C. 1988 Foam rheology: III Measurement of shear flow properties. *J. Rheol.* **32**, 69–92.

Kraynik, A. M., Reinelt, D. A. & van Swol, F. 2003 Structure of random monodisperse foam. *Phys. Rev.* E **67**, 031403.

Larson, R. G. 1997 The elastc stress in 'film fluids'. *J. Rheol.* **41**, 365–372.

Lauridsen, J., Twardos, M. & Dennin, M. 2002 Shear-induced stress relaxation in a two-dimensional wet foam. *Phys. Rev. Lett.* **89**, 098303.

Liu, A. & Nagel, S. R. 1998 Nonlinear dynamics. Jamming is not just cool any more. *Nature* **396**, 21–22.

Okuzono, T. & Kawasaki, K. 1995 Intermittent flow behavior of random foams: a computer experiment on foam rheology. *Phys. Rev.* E **51**, 1246–1253.

Okuzono, T., Kawasaki, K. & Nagai, T. 1993 Rheology of random foams. *J. Rheol.* **37**, 571.

Princen, H. M. 1983 Rheology of foams and highly concentrated emulsions : I. Elastic properties and yield stress of a cylindrical model system. *J. Colloid Interface Sci.* **91**, 160–175.

Reinelt, D. A. 1993 Simple shearing flow of three-dimensional foams and highly concentrated emulsions with planar films. *J. Rheol* **37**, 1117–1139.

Reinelt, D. A. & Kraynik, A. M. 1996 Simple shearing flow of a dry Kelvin soap foam. *J. Fluid Mech.* **311**, 327.

Reinelt, D. A. & Kraynik, A. M. 2000 Simple shearing flow of dry soap foams with tetrahedrally close-packed structure. *J. Rheol.* **44**, 453.

Rouyer, F., Cohen-Addad, S., Vignes-Adler, M. & Holler, R. 2003 Dynamics of yielding observed in a three-dimensiomal aqueous dry foam. *Phys. Rev.* E **67**, 021405.

Rouyer, F., Cohen-Addad, S. & Holler, R. 2005 Is the yield stress of aqueous foam a well-defined quantity? *Colloids Surfaces* A **263**, 111–116.

Sollich, P., Lequeux, F., Hébraud, P. & Cates, M. E. 1997 Rheology of soft glassy materials. *Phys. Rev. Lett*. **78**, 2020.

Viasnoff, V. & Lequeux, F. 2002 Rejuvenation and overaging in a colloidal glass under shear. *Phys. Rev. Lett*. **89**, 065701.

Vincent-Bonnieu, S., Hohler, R. & Cohen-Addad, S. 2006 Slow viscoelastic relaxation and aging in aqueous foam. *Eoruphys. Lett*. **74**, 533–539.

Wang, Y., Krishan, K. & Dennin, M. 2006 Impact of boundaries on the velocity profiles in bubble rafts. *Phys. Rev*. E **73**, 031401.

Weaire, D. & Hutzler, S. 1999 *The Physics of Foams*. Clarendon.

Weaire, D. & Kermode, J. P. 1983 Computer simulation of a two-dimensional soap froth I. Method and motivation. *Phil. Mag*. B **48**, 245–259.

Weaire, D. & Kermode, J. P. 1984 Computer simulation of a two-dimensional soap froth II. Analysis of results. *Phil. Mag*. B **50**, 379–395.